Lawrence Berkeley National Laboratory
Recent Work

Title
AN ANALYSIS OF THE HYDRODYNAMICS OF ALUMINUM REDUCTION CELLS

Permalink
https://escholarship.org/uc/item/0081t7mp

Authors
Moreau, R.
Evans, J.W.

Publication Date
1984

eScholarship.org Powered by the California Digital Library
University of California

LBL-17126
Preprint c.2

Lawrence Berkeley Laboratory
UNIVERSITY OF CALIFORNIA

RECEIVED
LAWRENCE
BERKELEY LABORATORY
APR 17 1984
LIBRARY AND
DOCUMENTS SECTION

Materials & Molecular Research Division

Submitted to the Journal of the Electrochemical Society

AN ANALYSIS OF THE HYDRODYNAMICS OF ALUMINUM REDUCTION CELLS

R. Moreau and J.W. Evans

January 1984

TWO-WEEK LOAN COPY

This is a Library Circulating Copy which may be borrowed for two weeks. For a personal retention copy, call Tech. Info. Division, Ext. 6782.

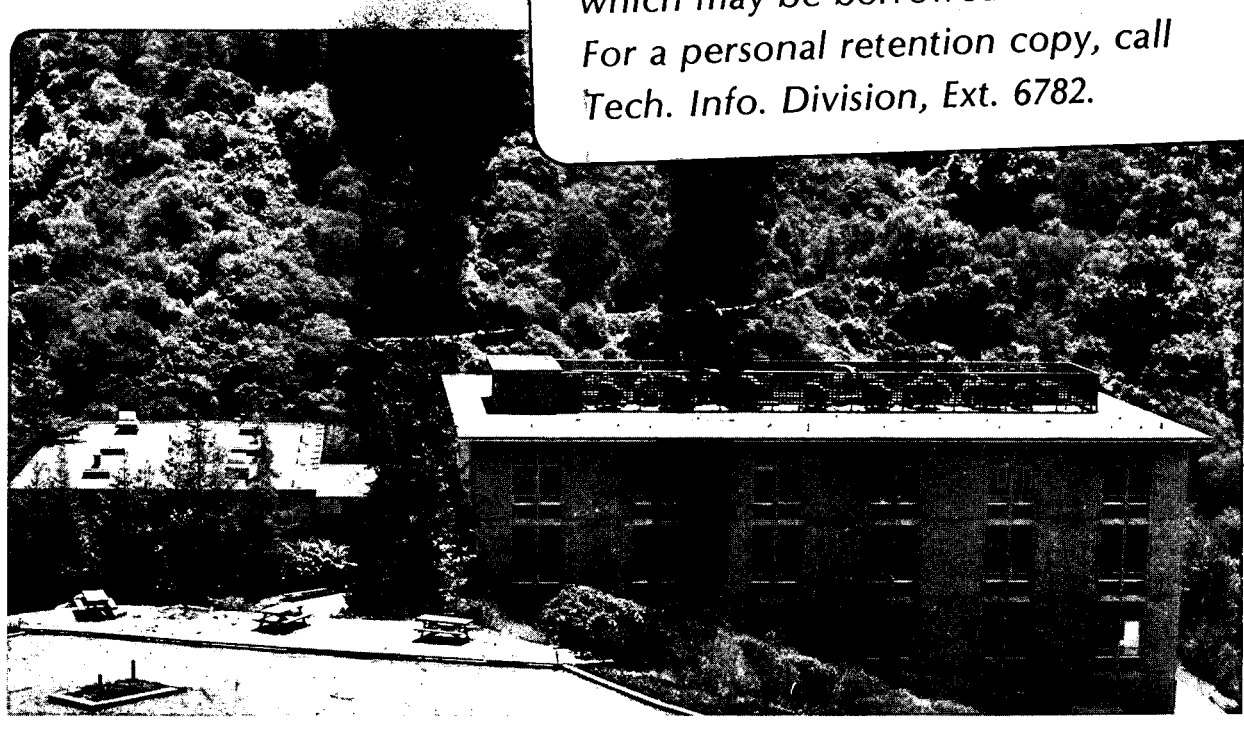

Prepared for the U.S. Department of Energy under Contract DE-AC03-76SF00098

LBL-17126
c.2

DISCLAIMER

This document was prepared as an account of work sponsored by the United States Government. While this document is believed to contain correct information, neither the United States Government nor any agency thereof, nor the Regents of the University of California, nor any of their employees, makes any warranty, express or implied, or assumes any legal responsibility for the accuracy, completeness, or usefulness of any information, apparatus, product, or process disclosed, or represents that its use would not infringe privately owned rights. Reference herein to any specific commercial product, process, or service by its trade name, trademark, manufacturer, or otherwise, does not necessarily constitute or imply its endorsement, recommendation, or favoring by the United States Government or any agency thereof, or the Regents of the University of California. The views and opinions of authors expressed herein do not necessarily state or reflect those of the United States Government or any agency thereof or the Regents of the University of California.

Submitted to the Journal of the Electrochemical Society, January 1984

AN ANALYSIS OF THE HYDRODYNAMICS OF ALUMINUM REDUCTION CELLS

R. Moreau, Professor
G.i.s MADYLAM, CNAS, Institut de Mecanique de Grenoble
Institut National Polytechnique de Grenoble
B.P. 68, 38402 Saint-Martin d'Heres Cedex, France

and

J. W. Evans, Professor of Metallurgy*
Department of Materials Science and Mineral Engineering
University of California, Berkeley
and
Materials and Molecular Research Division
Lawrence Berkeley Laboratory
Berkeley, California 94720

*To whom correspondence should be addressed.

ABSTRACT

An investigation of the flow of the two superposed liquids (the electrolyte and the molten aluminum) and of the interface shape has been carried out with the intention of revealing the main mechanisms and to clarify the hydrodynamic behavior of Hall-Héroult cells. The wide channels present around the anodes and between the two anodes rows in modern cells appear responsible, in the final analysis, for the electrolyte motion. The horizontal component of the current density in the aluminum layer largely determines the interface shape. It can also drive an organized motion when it is not a pure gradient. Two main ideas are at the source of this theory; i) the shallow depth of the fluid layers (compared with their horizontal dimensions) justifies an approximation of zero inertia, and ii) a linear approximation is proposed for the horizontal shear stresses. This almost explicit theory results in predictions that are not completely realistic, but it is shown how certain features of actual cell behavior can be revealed.

INTRODUCTION

There is considerable interest in better understanding the general behavior of Hall-Héroult cells, because these large devices, in which aluminum oxide is reduced electrolytically to produce molten metal, are known as the major energy consumer in the production of aluminum from its ores. For a full description of these cells the reader is referred to Lympany, Evans and Moreau (1). For the sake of brevity, it will only be mentioned that the electric current coming from the anodes (see fig. 1) has to pass first through a horizontal liquid layer, the electrolyte (often known as "cryolite") before entering into the molten aluminum layer (where it is partially redirected in the horizontal direction), and thence through the carbon lining and into the collector bars.

Electromagnetics, hydrodynamics, heat and mass transfer, as well as electrochemistry, enter immediately into any complete description of the cell. Indeed, magnetohydrodynamic effects are responsible for the motion and the turbulence of the two liquids, and play a significant role in determining the current efficiency. In recent work (2) the development of a mathematical model, based on general equations of electromagnetics and hydrodynamics, has been attempted in order to compute the main behavior of these cells. The objective was to build a convenient tool for conception of new cells with better efficiency (3).

It has, however, been recently realized that the two-dimensional Navier-Stokes equations and the usual turbulence modelling (k-ε) could not describe the true mechanisms involved in the motion of the two thin liquid layers. Using the k-ε model for turbulence in a supposed two-dimensional flow leads to neglect of the vertical transport of momentum, and this is unrealistic in this configuration where it is, in fact, dominant over the horizontal one. Besides, a purely two-dimensional schema could not take into account the presence of channels between the anode blocks

and around the cell periphery. These have, however, a strong influence on the flow of the electrolyte because they connect this flow with the atmospheric pressure, almost without head losses.

It is the purpose of this paper to propose a new basis of approximations to the hydrodynamics of the two superposed liquids, and to develop a better understanding of the influence of each parameter on the fluid flows and the interface shape. To do this, the concept of an ideal cell in which the electromagnetic forces are pure gradients, is introduced. As a consequence the cryolite is the only moving fluid. The pressure differences between the two liquids in different motion vary from one place to another, and this is responsible for the shape of the interface. It is also shown that second order effects can easily be superimposed on this state of reference predicted for the ideal cell, and an example is treated.

Each liquid layer may be characterized by its vertical thickness (under the anodes), H, its length, 2a, and its width, 2b. It appears convenient to introduce also a typical horizontal length scale, L, which can be either a or b or some combination of them, in order to characterize the thinness of the layer by the ratio H/L. The thickness H is of the order of 0.04m in the cryolite and 0.16 m in the aluminum. In typical modern cells, L may be of the order of 4 m, so that H/L is of the order of 10^{-2} in the cryolite and 4.10^{-2} in the aluminum. The smallness of H/L is of prime importance in the justification of the approximations proposed in section I. Other important orders of magnitude are the typical electric current ($\simeq 2.10^{5}$A) and the current density $j_o (\simeq 6.10^{3} Am^{-2})$.

The coordinates are defined in fig. 2, with x in the long horizontal axis and y in the small one. The z axis is along the upward vertical with its origin at the mean level of the interface between cryolite and aluminum. To illustrate the results, all the numerical computations have been done with a cell whose aspect ratio was a/b = 2. Unit vectors are denoted $\bar{e}_x$, $\bar{e}_y$, $\bar{e}_z$.

I. BASIC EQUATIONS AND APPROXIMATIONS

I.1 The relevant magnetic Reynolds number

The question of a possible influence of the velocities in the two superposed liquids on the magnetic field has often arisen. Clearly the relevant magnetic Reynolds number characterizing this effect must be the ratio between the diffusion time of the magnetic field through the whole cell and the transit time of the fluid elements LV^{-1}. In the idealized configuration of a thin layer of conducting material located between two insulating media, any disturbance would diffuse instantaneously through these media, so that its diffusion time would be $\mu\sigma H^2$ (μ and σ denote the permeability and the electrical conductivity of the conducting layer). The situation with which we are concerned is more complex because the media above and below the aluminum layer are conducting: they are thick (let H^* denote their total thickness) and they are conducting (let σ^* denote their conductivity). Forgetting the extremely short diffusion through the electrolyte layer, the total diffusion time through the cell may be estimated as $\mu (\sigma H^2 + \sigma^* H^{*2})$. Therefore the relevant magnetic Reynolds number is:

$$(1) \qquad R_m = \mu\sigma VL \cdot \frac{H^2}{L^2} \left(1 + \frac{\sigma^* H^{*2}}{\sigma H^2}\right)$$

It appears that, although $\mu\sigma VL$ may be of the order of a few units, H^2/L^2 is extremely small ($\simeq 3.10^{-4}$). This means that the vertical diffusion time through the aluminum layer is extremely small compared with the transit time. Besides, the ratio σ^*/σ is sufficiently small ($\simeq 2.10^{-3}$) to also render negligible the diffusion time through the electrodes. Then it may be concluded that the classical approximation of a zero magnetic Reynolds number is valid.

I.2. The "shallow water" approximation

Because of the shallowness of the two liquid layers and because of the very active mixing due to turbulence and to gas bubbles generated at the anode, the interest is essentially in describing the mean horizontal motion. If $\bar{u}_H$ denotes the horizontal velocity field, the definition of this mean motion is:

$$(2) \qquad \langle \bar{u}_H \rangle = 1/H \int_{-H}^{o} \bar{u}_H dz$$

The equations for such a two-dimensional flow are:

$$(3) \qquad \bar{\nabla}_H \cdot \langle \bar{u}_H \rangle = 0$$

$$(4) \qquad \rho \langle \left(\bar{u}_H \cdot \bar{\nabla}_H\right) \bar{u}_H \rangle = - \bar{\nabla}_H \langle p \rangle + \langle \left(\bar{j} \times \bar{B}\right)_H \rangle + \frac{\partial}{\partial x_i} \left(\eta_e \frac{\partial}{\partial x_i} \langle \bar{u}_H \rangle \right) - \frac{\bar{\tau}}{H}$$

The subscript H stands for the horizontal vectors or operators, so that $\bar{\nabla}_H = \left(\frac{\partial}{\partial x}, \frac{\partial}{\partial y}, 0 \right)$ and p denotes the pressure, ρ the density, η_e the effective viscosity, and $\bar{\tau}$ the sum of the shear stresses at the top and bottom of the fluid layer.

To appreciate the consequences of the small values of H/L, let us write Equation (4) in a non-dimensional form. Since the driving mechanism is the difference between the Lorentz forces and the pressure gradient, it is convenient to introduce the non-dimensional pressure

$$P = \frac{p}{\mu j_o^2 L^2} \quad \text{and the velocity scale} \quad V = \left(\frac{\mu j_o^2 L H}{p} \right)^{1/2}.$$

Then with $X_i = \frac{x_i}{L}$, $\bar{U} = \frac{\bar{u}_H}{V}$, $T = \frac{\bar{\tau}}{\rho V^2}$, and $\bar{F} = \frac{\langle (\bar{j} \times \bar{B})_H \rangle}{\mu j_o^2 L}$

the non-dimensional equation is:

$$(5) \qquad \frac{H}{L} \left(\bar{U} \cdot \bar{\nabla}_H\right) \bar{U} = - \bar{\nabla}_H P + \bar{F} - \bar{T} + \frac{H}{L} \frac{\nu}{VL} \frac{\partial}{\partial X_i} \left(\frac{\eta_e}{\eta} \frac{\partial \bar{U}}{\partial X_i} \right)$$

With the typical values of H/L previously mentioned, for modern cells, with current of the order of 2.10^5 amps, V is of the order of 0.1 $m.s^{-1}$ and the Reynolds number VL/ν is of the order of 4.10^5. Therefore, even if η_e is much higher than the molecular viscosity η because of the intense mixing present in each liquid, it is clear that the two-dimensional friction (or the horizontal transport of momentum) cannot compete with the Lorentz forces. Inertia also appears unable to balance the driving forces. Consequently the dominant equilibrium is between the difference $\overline{F}-\overline{\nabla}_H P$ (which is not exactly zero as will be seen later) and the friction on the horizontal boundaries $\overline{T}$. Then the equations for the two-dimensional flow of each liquid reduce to:

$$\overline{\nabla}_H \cdot \overline{U} = 0 \qquad (6)$$

$$\overline{T} = \overline{F} - \overline{\nabla}_H P \qquad (7)$$

Of course this approximation still needs an assumption for the relation between the drag $\overline{T}$ and the velocity $\overline{U}$. Two ideas suggest that a linear expression i.e.

$$\overline{T} = \kappa \overline{U} \qquad (8)$$

could be quite plausible, and certainly better than a quadratic expression (as in turbulent duct flows). One idea is the previously established fact that inertia is negligible in these shallow layers of liquids. The other derives from the fact that the typical scale of random eddies responsible for the vertical transport of momentum is H which is much smaller than the typical horizontal length scale of the mean motion L. The situation appears then more similar to the kinetic theory of gases (with a mean free path much smaller than the macroscopic scales) than usual

turbulent flows (with an integral scale of the same order as the length scales of the mean flow). We will therefore retain this very simple expression (8). It will be seen that it has also the advantage of allowing a clear illustration and understanding of the mechanism of stirring in each liquid.

I.3. The influence of the cryolite channels

Since the cryolite is a poor conductor, compared to the carbon electrodes, the fraction of the electric current crossing the channels between the anode blocks may be neglected. Then the flow in these channels behaves like an open channel flow, having the capability of exchanging mass and momentum with the neighboring two-dimensional flow underneath the anodes. In spite of this mass exchange the mean flow in a straight channel is such that the pressure variation in the cross-section follows the law of hydrostatics. However, pressure differences develop underneath the anodes, in order to partially balance the Lorentz forces according to Equation (7). Because of the continuity of pressure between the cryolite layers and the channels, pressure gradients may also exist in the channels where they would necessarily drive some flow and be balanced by friction and momentum transport.

Let S denote the area of the cross-section, P the wet perimeter, and q the flow rate which is a function of the abcissa δ along the channel. If u_n and u_δ stand for the outward normal and tangential velocity components of the two-dimensional cryolite flow along the anode edge, and if τ_w denotes the wall shear stress, the mass and momentum conservation equations can be written:

$$(9) \qquad \frac{dq}{d\delta} = u_n H$$

$$(10) \qquad \frac{d}{d\delta}\left(\rho \frac{q^2}{S}\right) - \rho u_n u_\delta H = - S \frac{dP}{d\delta} - P\tau_w$$

Because of the variations of the liquid depth, themselves related to the

topology of the free surface and of the interface, and because of possible variations in the shape of the solidified ledge of cryolite (for the peripheral channel), the parameters S and P may slowly vary from one place to another. However, in this theory they are supposed to be constant for the sake of simplicity. The wall friction τ_w is assumed to follow the usual quadratic law.

$$(11) \qquad \tau_w = \lambda \rho \frac{q^2}{S^2}$$

where the friction coefficient λ has still to be estimated.

Introducing the non-dimensional quantities

$$(12) \qquad Q = \frac{q}{VLH} \qquad t = \frac{\delta}{L} \qquad U_n = \frac{u_n}{V} \qquad \text{etc.}$$

equations (10) and (11) reduce to

$$(13) \qquad \frac{H^3 L}{S^2} \frac{dQ^2}{dt} - \frac{H^2}{S} U_n U_t = - \frac{dP}{dt} - \frac{P L^2 H^3}{S^3} \lambda Q^2$$

This equation exhibits three dimensionless numbers, essentially depending on the geometry, which characterize the three possibilities of balancing any longitudinal pressure gradient: momentum transport along the chanel, or toward the horizontal layer of cryolite under the anodes, and friction.

There are two kinds of channels: the wide ones present around the cell periphery (or between the two rows of anodes in modern cells with automatic feeding of alumina), and the narrow ones between the anode blocks, 3 or 4 cm apart. In the wide channels typical values S = 0.5 m^2 and P = 0.6 m seem to be realistic and provide the following orders of magnitude:

$$\frac{H^3 L}{S^2} \simeq 10^{-3}, \quad \frac{H^2}{S} \simeq 3.10^{-3}, \quad \frac{P L^2 H^3}{S^3} \lambda \simeq 5.10^{-3} \lambda$$

The consequence of these very small values is that any pressure difference along the large channels could not be balanced. In other words the channels are so large that their free surface must be horizontal. Therefore the presence of these large channels is dictating the striking boundary condition that P must be constant at the edge of the anode rows.

In the narrow channels, with P of the same order but S smaller ($\simeq 0.1\ m^2$), the non-dimensional numbers have the following orders of magnitude:

$$\frac{H^3 L}{S^2} \simeq 2.5 \times 10^{-2}, \qquad \frac{H^2}{S} \simeq 1.6 \times 10^{-2}, \qquad \frac{\rho L^2 H^3}{S^3}\lambda \simeq 0.6\lambda$$

It still appears that the momentum transport could not balance any pressure gradient. But the situation is not as simple with regard to friction because λ is very difficult to estimate. If these channels behaved like ordinary turbulent duct flows, λ would be in the range 10^{-2} to 10^{-1}. But the intense bubbling activity (carbon dioxide evolved from the anodes), particularly important in these channels because of their narrowness, would increase λ by a few orders of magnitude. One has therefore to accept the idea that some pressure differences (and variations in the height of the free surface) can take place. They could be modelled by the equation

$$(14) \qquad \frac{dP}{dt} + \frac{\rho L^2 H^3}{S^3}\lambda Q^2 = 0$$

with a convenient guess for the λ coefficient. Since it is one of the aims of this paper to simplify rather than to inspect all the details, it will be considered that the friction term is dominant over the pressure gradient, as it would be if the gap between the anode blocks were smaller ($\lesssim 1$ cm). Then Equation (14) reduces to $Q = 0$,

and these channels may be ignored in this asymptotic limit.

It has still to be noticed that the cryolite channels have another consequence in allowing U_n to be non-zero at the boundary of the layer underneath the anodes. The flow rate in these channels Q follows from relations (8) and (12). This is to be contrasted with the aluminum layer, at the border of which no such channels exist; U_n has to be zero at the aluminum boundary, but no restriction applies on the pressure.

I.4. The interface equation

In each liquid the vertical variation of pressure is of the form

$$(15) \qquad p = - \rho_i g z + f_i(x,y)$$

where z is the upward vertical, g gravity, and where the values 1 and 2 will be used for the subscript i respectively in the cryolite and the aluminum. The functions $f_1(x,y)$ and $f_2(x,y)$ can only be determined by solving first Equation (6) and (7) in each liquid with the relevant boundary conditions. Then the continuity of pressure at the interface $z = z_o$ gives the equation of this surface:

$$(16) \qquad (\rho_2-\rho_1)\, g z_o = f_2(x,y) - f_1(x,y)$$

II. A FIRST MODEL FOR AN IDEAL CELL

II. 1. Assumptions for currents and magnetic fields

In each cell the current density has a specific distribution depending on parameters like the geometry of each anode block, the particular design of the risers, the position of the collector bars, etc. The magnetic field also is dependent on many parameters (the effect of which is not easily taken into account

explicity), such as the position of the cell in a pot line or the shielding effect of the steel shell surrounding the cell. Therefore any distribution of the Lorentz forces $\overline{j} \times \overline{B}$ which could be considered as sufficiently exact for a given cell would certainly be imprecise for many others. Since a main goal of this study is to reach a general understanding of the hydrodynamics of cells, it has been choosen to use some "ideal" distributions of $\overline{j}$ and $\overline{B}$, rather than to compute them. (Notice that even computed distributions would not be "exact.") Of course such distributions have to be in agreement with some first order requirements such as the respective positions and voltages of the anodes, the two liquids, the carbon cell lining, and the collector bars. They should also contain a small number of parameters which are to be adjusted by comparison with measurements or computed distributions such as those of Lympany and Evans [3]. The first approximation developed in this section is based on the following assumptions:

i) The j_x component in the long horizontal direction is taken to be zero since the collector bars usually drive the horizontal current in the y direction.

ii) Because of the very small electrical conductivity and depth of the cryolite layer, the current density is supposed purely vertical and uniform in this liquid ($j_z = -j_o$).

iii) In the aluminum the distribution of the current density is taken as:

(17) $$j_y = j_1 \frac{y}{H}, \qquad j_z = -j_o + j_2 \frac{z}{H}$$

where H is the depth of the aluminum layer; the level variations of the interface are neglected for electromagnetic calculations

iv) The magnetic field of all the external conductors is neglected by comparison with that of the internal current, which is itself assumed purely horizontal ($B_z << B_x, B_y$) and without variations with z in the gap of interest. Then the vector potential is purely vertical:

(18) $$B_x = \frac{\partial A}{\partial y}, \qquad B_y = -\frac{\partial A}{\partial x}$$

and follows Ampere's law:

(19) $$\nabla_H^2 A = -\mu j_z$$

Clearly these assumptions are open to discussion and improvements. For instance section III shows an example of such an improvement obtained by adding a supplementary term and a supplementary parameter in relations (17) in order to include a new effect. Indeed these relations (17) may be considered as the simplest combination of two conservative fields allowing the study of the influence of the horizontal current density via the parameter j_1. Assumption (iv) may be understood as a tool to isolate the internal characteristics of the cell from external characteristics such as the arrangement of risers and collectors. Of course an explicit approximation of the magnetic field induced in the two liquids by the external conductors could be added in Equations (18) and (19). But it follows from computed results (3) that this external magnetic field is definitely a second order effect (a few gauss compared to 50 gauss due to internal current).

Equation (19), together with $\nabla_H^2 A = 0$ outside the rectangle 2a x 2b, and the conditions of continuity of A and its two first derivatives on the boundary, has a solution of the form:

(20) $$A = (j_o + j_1 \frac{z}{H}) \mu G(x,y)$$

where G(x,y) is completely determined by equation

(21) $$\nabla_H^2 G = \begin{cases} 1 & \text{inside the rectangle} \\ 0 & \text{outside the rectangle} \end{cases}$$

and by the continuity conditions. This solution, analogous to the distribution of the electric potential created by a charge density which is uniform in a rectangle and zero outside, is explicity known (Durand, see Appendix A).

It follows from these assumptions that the Lorentz force has a simple expression in terms of A:

$$\bar{j} \times \bar{B} = j_z \bar{\nabla}_H A = -\frac{1}{\mu}\nabla_H^2 A \cdot \bar{\nabla}_H A \tag{22}$$

Since we only need its mean value in each fluid layer, let us write:

$$\bar{j} \times \bar{B} = -\mu j_o^2 C \bar{\nabla}_H G \tag{23}$$

where C is a non-dimensional parameter representing the influence of the horizontal current j_y. It follows from our assumptions that C = 1 in the cryolite layer whereas in the aluminum it has the value

$$C = 1 - \frac{j_1}{j_o} + \frac{1}{3}\frac{j_1^2}{j_o^2} \tag{24}$$

II.2 Motion and pressure in the cryolite layer

The non-dimensional form of Equation (23) to use with Equation (6), (7) and (8) in the electrolyte is $\bar{F} = -\bar{\nabla}_H G$. Therefore, the motion equations in this layer are

$$\bar{\nabla}_H \cdot \bar{U}_1 = 0 \tag{25}$$

$$\kappa_1 \bar{U}_1 = -\bar{\nabla}_H (P_1 + G) \tag{26}$$

Taking the divergence of (26) yields the equation for the pressure distribution

$$\nabla_H^2 P_1 = -1 \tag{27}$$

The solution satisfying the boundary condition that $P_1 = 0$ at the boundary of a

rectangle is explicitly known; it is analogous to the temperature distribution in a rectangle with uniform heat production and boundaries at a constant temperature (Carslaw and Jaeger, see Appendix A).

This solution is illustrated in Figure 3, and may be compared with the solution of Equation (21) for G. It is clear that the boundary condition, imposing a stricter condition on P_1 than on G, makes all the difference between these two functions and prevents the two gradients from canceling each other. To emphasize this difference, which is the key to the mean flow in the cryolite, one could say that because of the presence of the wide channels, the isobars resembles rectangles, whereas the lines G = Constant look rather like circles.

The influence of a wide central channel appears very important when Figure 3a is compared with Figure 3b where a center channel has been introduced. The center channel has essentially two main effects.

i) There are two symmetrical pressure domes, one under each anode row, when there is a wide central channel, rather than one bigger dome centered in the middle of the cell when no wide central channel is present (Figure 3a).

ii) In forcing $P_1 = 0$ at the center and along the x axis as well as at the boundary, the presence of a wide central channel reduces the pressure differences and the pressure forces, for the same given value of the Laplacian (by a factor 3.7 in the computed case).

It is straight-forward to deduce the velocity field from (26) when P_1 and G are known. Figure 4 shows the streamlines of this potential flow as deduced from equations

$$(28) \qquad \kappa_1 U = \frac{\partial \Psi}{\partial y} = - \frac{\partial}{\partial x} (P_1 + G)$$

$$\kappa_1 V = \frac{\partial \Psi}{\partial x} = - \frac{\partial}{\partial y} (P_1 + G)$$

The influence of a wide central channel again appears dramatic since the nature of

the main flow is completely different between Figure 4a and 4b. It is, however, easy to interpret these flow patterns: When there is no central channel the same pressure difference does exist along the small and the large axes, but the inward electromagnetic forces are dominant along the large axis whereas the outward pressure gradient is dominant along the small axis. When a wide central channel is present, the general reduction of pressure differences makes the electromagnetic forces predominant everywhere and provides a velocity field almost parallel to the force field.

It is also of interest to notice that the value of the stream function Ψ is 3.5 times greater with,than without,a central channel in the computed case, and that the place where Ψ is maximum is not at all the same in the two cases. Also the direction of the mean flow in the peripheral channel is changed when a wide central channel is present.

These predictions could be checked with direct observations on real cells since the wide channels are more accessible than the shadow of the anode (6). The flow rate in these channels is easily deduced from the values of Ψ at the boundary:

$$(29) \qquad q = \left(\frac{\mu j_o^2 H^3 L^3}{\rho}\right)^{1/2} \frac{\Psi}{K_1}$$

and seems to be the first quantity to be checked with measurements.

It is remarkable that in this inertia free approximation it is not necessary to give a numerical value to the friction coefficient K_1 to find out the flow pattern. This is, however, necessary to get some numerical value of the flow rates in the channel from Equation (29). Inversely, this relation could be used as an empirical way to determine K_1.

II.3. Pressure in the aluminum and interface shape

In the aluminum layer, the motion equations are very similar to (25) and

(26) with the only difference that the velocity potential is now $P_2 + CG$. The important feature is the absence of channels or anything equivalent. The force distribution (23) is assumed to be valid everywhere, and the depth of the aluminum layer is assumed to be uniform. Then the only boundary condition demands that the normal component of the velocity be zero on the edge of the rectangle. The only irrotational plane motion satisfying this condition is $\overline{U}_2 \equiv 0$. As a consequence, the pressure distribution in the aluminum is

$$p = -\rho_2 gz - \mu j_o^2 L^2 CG + \text{constant} \tag{30}$$

The analogous equation in the cryolite layer is

$$p = -\rho_1 gz + \mu j_o^2 L^2 P_1 \tag{31}$$

and it is straight-forward to deduce from (30) and (31) the interface equation

$$(\rho_2-\rho_1)gz_o = -\mu j_o^2 L^2 (P_1 + CG) + \text{constant} \tag{32}$$

Our choice that the z origin be at the mean level of the interface determines the constant, and the final equation of the interface is

$$\frac{(\rho_2-\rho_1)g}{\mu j_o^2 L^2} z = \overline{P_1 + CG} - (P_1 + CG) \tag{33}$$

where the upper bar is used to designate the average value in the rectangle.

Figures 5, 6, and 7 show the results for our cell of reference (aspect ratio: 2), with and without a wide central channel, and for two values of the parameter C. The unrealistic case C = 1 has interest only as a reference to illustrate the influence of the horizontal current in the aluminum when C is smaller than one. It appears that the predicted shape looks like a dome with deviations which are worthy of discussion.

To interpret these results, remember first that the overpressure which is developed under the anodes in the cryolite layer is the strongest when there is no central channel. Furthermore, the pressure differences which arise in the aluminum

layer are exactly those necessary to balance the electromagnetic forces. In particular, the smaller $|j_y|$ (C = 1), the larger $|j_z|$, and the higher these pressure differences. The general dome shape is due to the fact that the central overpressure is generally smaller in the cryolite than in the aluminum; therefore the only possibility to generate such a departure on a vertical line is to vary the height of the denser liquid. This is particularly clear along the boundaries of the rectangle where the interface is always like a dome, because p = Constant in the cryolite, whereas in the aluminum it has to be a maximum at the middle of each side and to be the smallest at the corners in order to balance the inward electromagnetic forces. Therefore one understands that in the four computed cases the dome is the most significant when C = 1 and when a large central channel is present. It is, on the contrary, the weaker when C = 0.5 and without any central channel.

From among the noticeable deviations from this dome shape, notice the central saddle or trough in the middle of a cell without a central channel. It comes from the fact that the central overpressure is higher in the cryolite than in the aluminum. It is remarkable that the depth of this trough increases when C decreases, thus illustrating the influence of increasing the horizontal current in the aluminum. Varying the coefficient C would also show that the lower point of the interface (still for a cell without central channel), which is at the corner when C = 1, moves along the small side to its middle and then along the large axis to the cell center as C decreases monotomically to its limit of 0.25 imposed by Equation (24).

III. EXAMPLE OF A SECOND ORDER IMPROVEMENT

III.1. Correction of the electromagnetic data

When expressions (17) are compared with plausible values such as those computed by Lympany and Evans (3), their linear variation with the coordinates does not seem to be correct for more than three-quarters of the cell width. It appears that in the outermost quarter some reduction should be introduced in relations (17).

This comes from the fact that the aluminum pool is wider than the anode. Indeed the geometry of the external boundary of the aluminum layer is in itself a difficult question. The key point is the shape and the position of the ledge of solidified electrolyte all around the cell. It is, of course, strongly dependent on the thermal behavior of the cell, and it exhibits important variations form one cell to another, as well as in a given cell during its life.

In this section consequences of this boundary phenomenon are studied as a disturbance of the reference state described in Section II. Because of the linearity of the motion equations (6), (7), and (8), this disturbance need not be supposed to be very small. However, the thickness of the region through which such a disturbance is concentrated is assumed to be small enough, so that ideas and techniques of the boundary layer theory apply.

The disturbance of the current density is supposed to take place in a plane (n,z), where n is the outward normal to the rectangle edge (Figure 2), and to have have the following distribution:

(34)
$$j_n = -j_2 \frac{\delta}{H} e^{n/\delta} , \quad j_z = j_2 \frac{z}{H} e^{n/\delta}$$

Clearly two new parameters (j_2 and δ) are thus introduced to characterize this disturbance. No restriction applies on j_2, but the thickness δ of the disturbed layer is supposed to be much smaller than the width of the rectangle, so that the derivative $\frac{\partial}{\partial t}$ may be neglected in comparison with $\frac{\partial}{\partial n}$, except in the vicinity of the corners where this theory fails.

The vector potential of the magnetic field may then be written

(35)
$$A = (j_o + j_1 \frac{z}{H}) \mu G(x,y) - \mu j_2 \delta^2 \frac{z}{H} e^{n/\delta}$$

where the last term (the correction to (20)) is the solution of the simplified form of Equation (19).

It follows that the mean value of the elctromagnetic forces in the aluminum layer is now:

$$(36) \qquad \langle \bar{j} \times \bar{B} \rangle = -\mu j_o^2 \left[C \bar{\nabla}_H G - D\{ e^{n/\delta}\, \bar{\nabla}_H G + \delta^2 \bar{\nabla}_H (e^{n/\delta}) \} + E\, \frac{\delta^2}{2} \bar{\nabla}_H\, (e^{2n/\delta}) \right]$$

where non-dimensional coefficients D and E, characterizing the importance of j_2, have the definitions

$$(37) \qquad D = \frac{j_2}{j_o}\ (-1/2 + 1/3\, \frac{j_1}{j_o}) , \qquad E = 1/3\, \frac{j_2^2}{j_o}$$

The two terms proportional to δ^2 in equation (36) can be neglected in comparison with $De^{n/\delta}\, \bar{\nabla}_H G$ which appears as the essential correction. Notice also that they are pure gradients and could not drive any aluminum motion. It is then interesting to notice the distribution of the curl of the forces:

$$(38) \qquad \bar{\nabla}_H \times \langle \bar{j} \times \bar{B} \rangle = \frac{\mu j_o^2 D}{\delta}\ e^{n/\delta}\, \frac{\partial G}{\partial t} \cdot \bar{e}_z$$

Since $\frac{\delta G}{\delta t}$ is zero at the middle of each side and increases or decreaes towards the corners as an odd function of the abcissa, it is clear that the flow driven along each side by this force has the directions and symetries shown on Figure 2.

III.2 The motion in the aluminum

Let us introduce the decomposition

$$(39) \qquad \bar{U} = \bar{U}_c + \bar{u}^* , \qquad \bar{P} = \bar{P}_c + \bar{p}^*$$

where $\bar{U}_c$ and $\bar{P}_c$ stand for the dimensionless values of $\bar{u}$ and p in the central core of the aluminum rectangle, and vary on the typical length scale L. The corrections u^* and p^* are concentrated in the boundary region along the edge and vary along the

normal on the short length scale δL. Clearly $\overline{U}_c$ and P_c are no longer the values determined in the reference state, since the flow driven in the boundary region by the electromagnetic forces has to recirculate in the central core. Dimensionless equations (6) to (8) then become:

(40) $$\overline{\nabla}_H \cdot \overline{U}_c = 0$$

(41) $$\kappa_2 \overline{U}_c = -\overline{\nabla}_H (P_c + CG)$$

(42) $$\overline{\nabla}_H \cdot \overline{u}^* = 0$$

(43) $$\kappa_2 \overline{U}^* = -\overline{\nabla}_H p^* + De^{n/\delta}\, \overline{\nabla}_H G$$

In the boundary region the normal component u^*_n is negligible compared to the tangential component u^*_t. Therefore, with the matching condition $p(n \to -\infty) = 0$, the normal projection of Equation (43) gives the disturbance of the pressure:

(44) $$p^* = D \int_{-\infty}^{n} e^{n/\delta} \frac{\partial G}{\partial n}\, dn = D\delta \left(\frac{\partial G}{\partial n}\right)_{n=0} e^{n/\delta}$$

Then after substitution of $\frac{\partial p^*}{\partial t}$, the tangential projection gives the u^*_t velocity component:

(45) $$\kappa_2 u^*_t = \frac{D}{\delta} \int_{-\infty}^{n} e^{n/\delta} \frac{\partial G}{\partial t}\, dn = D \left(\frac{\partial G}{\partial t}\right)_{n=0} e^{n/\delta}$$

Finally the continuity equation and the matching condition $u^*_n(n \to -\infty) = 0$ give the u^*_n velocity component:

(46) $$\kappa_2 u_n^* = -D\delta \left(\frac{\partial^2 G}{\partial t^2}\right)_{n=0} e^{n/\delta}$$

It follows from the two last expressions that the non-dimensional flow rate driven by the electromagnetic forces in the boundary regions is $\frac{D\delta}{\kappa_2}\left(\frac{\partial G}{\partial t}\right)_{n=0}$.

The core has essentially to feed these boundary regions. This demands

(47) $$U_{cn}(n=0) = D\partial \left(\frac{\partial^2 G}{\partial t^2}\right)_{n=0}$$

in order that the total normal velocity component be zero at the boundary. Therefore the molten aluminum cannot stay at rest in the core as in the reference state. The potential flow satisfying (40) and (41) may be determined in terms of a stream function Ψ_c. Taking account of the symetries, in the cell quarter $x>0$ and $y>0$ this stream function, whose definition is

(48) $$\kappa_2 U_{cx} = \frac{\partial \Psi c}{\partial Y} , \qquad \kappa_2 U_{cy} = -\frac{\partial \Psi c}{\partial X} ,$$

is completely determined by the Laplace equation $\nabla^2_H \Psi_c = 0$ together with the boundary condition

(49) $$\begin{cases} \Psi_c = 0 & \text{on the axes} \\ \Psi_c = -D\delta \left(\frac{\partial G}{\partial X}\right)_{y=b} & \text{on side AC} \\ \Psi_c = D\delta \left(\frac{\partial G}{\partial Y}\right)_{x=a} & \text{on side B} \end{cases}$$

Some typical streamlines shown on fig. 8 illustrate the main character of this flow. For the core flow the corners are source points from which comes the flow rate necessary to feed the boundary regions. And in return they are the sink points to which goes all the flow of the boundary regions. Of course this singularity of the corners is nothing but a consequence of the asymptotic character of this theory which is only rigorous in the limit of $\delta \to 0$.

It is also straightforward to calculate the pressure distribution. The velocity potential $\phi_c = P_c + CG$ which has also to satisfy the Laplace equation following (40) is completley determined by the Newmann boundary condition (47). Some typical potential lines are also shown on Figure 8. The pressure correction is proportional to $D\delta G$ and is therefore much smaller than the pressure differences found in the state of reference (proportional to CG). Therefore, it cannot introduce any important change into the interface topology. It is, however, interesting to notice that this second order effect tends to compensate for the differences of level found at the state of reference, since the higher pressure correction takes place in the corners and tends to raise these lowest points of the interface.

IV. REMARKS AND DISCUSSION

The hydrodynamics of Hall-Héroult cells have been the subject of many investigations since the pioneering work by Givry [7]. The fact that the governing mechanisms were still unclear, and that the numerical predictions [2] and [8] did not predict the same flow pattern, have given to this problem the reputation of being extremely difficult. In this context this paper introduces a new point of view and some simplifications which provide an important clarification. From two main approximations (the way to model the channels influence the cryolite flow, and the shallow water approximation) arises an almost elementary solution for an ideal cell. This solution may be seen as a first order solution and remains open to improvements. It shows that phenomena like the interface shape and the cryolite motion are controlled at the first order of approximation by the geometry of the channels between the anode blocks and around the cell, and by the distribution of the horizontal current in the aluminum layer.

This elementary theory has, however, still some weaknesses suggesting future work:

i) The analysis supposes that the channels are either very wide or very narrow, and that their width is not taken as a parameter. To remedy this first weakness, numerical solutions of the motion equations (6) to (8) together with relation (14) as a boundary condition at the edge of each anode block should be used in the cryolite (see Appendix B).

ii) Another resides in the fact that the idealized force distributions (23) or (36) do not coincide with those of a real cell. The remedy is obviously in the numerical computation of electric currents, magnetic fields, and force fields, as done by Evans, Zundelevich and Sharma [2]. It would permit the real distributions of $<(\overline{J} \times \overline{B})_H>$ to be introduced in the motion equations before computing the velocity fields.

iii) It must also be pointed out that this first investigation is only concerned with a steady state, which is assumed to coincide with an average of the actual unsteady states. The unsteadyness and the turbulence are only taken into account through the friction coefficients κ_1 and κ_2. To make significant progress in the understanding of the cell's behavior it would be now important to study the mechanisms of instability of the interface. In this context it is felt that the present concept of an ideal cell with an elementary steady state of reference offers the necessary basis into which small disturbances could be introduced and studied.

iv) Assumption (8) that $\overline{T}$ is proportional to the local velocity can only be justified in an ideal cell with mean velocities much smaller in the aluminum than in the cryolite. For cells with rotational Lorentz forces, relation (8) could be generalized under the form

$$(50) \quad \begin{cases} \overline{T}_1 = \kappa_1 \overline{U}_1 + \gamma \overline{U}_2 \\ \overline{T}_2 = \kappa_2 \overline{U}_2 + \gamma \overline{U}_1 \end{cases}$$

Such expressions that retain the linearity of the problem would not really make the

numerical computation more difficult. The interest in their use would be to introduce some coupling between the two fluid flows. This coupling should not be ignored since each liquid tends to drive the neighboring one in the direction of its own motion.

v) In itself this theory cannot give any idea of the numerical values of coefficients κ_1, κ_2 and γ. It is the hope of the authors that some comparison of measurements such as those made by Johnson [6] with numerical predictions deduced from equations of Appendix B could provide a good estimation for these parameters.

This work was supported by the Assistant Secretary for Conservation and Renewable Energy, Office of Energy Systems Research, Energy Storage Division of the U. S. Department of Energy under Contract Number DE-AC03-76SF00098.

APPENDIX A: Explicit solutions of equations (21) and (31)

With notations defined in fig. 9 and $c = (a^2 + b^2)^{1/2}$, the solution of Eq. (21), such that the functions G (x,y) and its two first derivatives be continuous on the edge of the rectangle, may be written:

$$2\pi G = h_1 h_2 \operatorname{Log}\left(\frac{r_1}{c}\right) + h_2 h_3 \log\left(\frac{r_2}{c}\right) + h_3 h_4 \log\left(\frac{r_3}{c}\right) + h_4 h_5 \log\left(\frac{r_4}{c}\right)$$

$$+ 1/2 \left[h_1^2 (\beta_1 - \beta_4) + h_2^2 (\beta_2 - \beta_1) + h_3^2 (\beta_3 - \beta_2) + h_4^2 (\beta_4 - \beta_3) \right] \tag{A1}$$

$$+ \frac{\pi}{4} \left[h_1^2 + h_2^2 + h_3^2 + h_4^2 \right] .$$

The last term is a particular solution of the Poisson equation $\nabla^2 G = 1$. The other terms are solutions of Laplace equation $\nabla^2 G = 0$. At the origin of coordinates the value of G is:

$$G(o) = \frac{1}{2\pi} \left[\pi b^2 + 2(a^2 - b^2) \arctan\left(\frac{b}{a}\right) \right] \tag{A2}$$

It can be subtracted from (A1) to get a zero value at the origin.

The solution of eq. (27) such that P_1 be zero at the edge of the rectangle is:

$$P_1 = \frac{a^2 - x^2}{2} - \frac{16a^2}{\pi^3} \sum_{n=0}^{\infty} \frac{(-1)^n \cos[(2n+1)\pi x/2a] \cosh[(2n+1)\pi y/2a]}{(2n+1)^3 \cosh[(2n+1)\pi b/2a]} \tag{A3}$$

APPENDIX B: Procedure for computation of velocity fields and interface shape in real cells.

When the distributions of the force fields $\overline{F}_1$ and $\overline{F}_2$ have been computed, the equations to solve to determine the velocity and pressure distributions in the two liquids are (6) and (7) with expressions (8) or (50) for the drag $\overline{T}_i$.

In the cryolite the boundary condition to use on the edge of each anode block is:

$$(B1)\quad \begin{cases} P_1 = 0 & \text{in wide channels} \\ \dfrac{dP_1}{dt} + \Lambda Q^2 = 0 & \text{in narrow channels} \end{cases}$$

where $Q = \int U_n(n=0)\, dt$ stands for the dimensionless flow rate in the channels, and where

$$\Lambda = \frac{\rho L^2 H^3}{S^3}\lambda$$

denotes the dimensionless friction coefficient. Taking the divergence of Equation (7) gives a Poisson equation, the solution of which $P_1(x,y)$ is completely determined by (B_1). Then (7) gives:

$$(B2)\quad \kappa_1 \overline{U}_1 + \gamma \overline{U}_2 = \overline{F}_1 - \overline{\nabla}_H P_1$$

In the aluminum the boundary condition to use on the edge of the metal pool is $U_n = 0$. Taking the curl of the motion equation and eliminating $\overline{\nabla}_H \times \overline{U}_1$ with (B2) gives:

$$(B3)\quad \left(\kappa_2 + \frac{\gamma^2}{\kappa_1}\right)\overline{\nabla}_H \times \overline{U}_2 = \text{curl}\ \overline{F}_2 - \frac{\gamma}{\kappa_1}\ \text{curl}\ \overline{F}_1$$

The technique to solve Equation (B3) for a conservative velocity field ($\bar{\nabla}_H \cdot \bar{U}_2 = 0$) is quite straight-forward. A stream-function is usually introduced, and appears to be determined by a Poisson equation together with the boundary condition that $U_n = 0$ at the edge of the aluminum pool. The velocity field $\bar{U}_2$ is thus determined. Then (B_2) gives the velocity field $\bar{U}_1$, and the pressure distribution $P_2(x,y)$ follows from the motion equation.

Finally the interface shape is given by:

$$\text{(B4)} \qquad \frac{(\rho_2-\rho_1)gz_o}{\mu j_o^2 L2} = P_2(x,y) - P_1(x,y) - (\bar{P}_2-\bar{P}_1).$$

FIGURE CAPTIONS

1. Sectioned view of a Hall-Héroult cell as seen looking in the long horizontal direction.

2. Coordinates and main notations in a typical horizontal plane.

3. Potential lines (G = Const.) of the $\langle \bar{j} \times \bar{B} \rangle$ force field, and pressure lines (P = Const.)

   a) for a cell without central channel

   b) for a cell with central channel

4. Streamlines of the cryolite flow underneath the anode

   a) for a cell without central channel

   b) for a cell with central channel

5. Interface contour lines when C = 1 ($j_1 = 0$, i.e. no horizontal current in the aluminum)

   a) for a cell without central channel

   b) for a cell with central channel

6. Interface contour lines when C = 0.5 ($j_1/j_o = 0.634$)

   a) for a cell without central channel

   b) for a cell with central channel

7. Interface shape in the four computed cases

   a) C = 1, without central channel

   b) C = 1, with central channel

   c) C = 0.5, without central channel

   d) C = 0.5, with central channel

8. Typical streamlines of the core flow feeding the side boundary layers in the aluminum pool.

9. Definition of notations used in equation A1.

FIG. 1 Sectioned view of a Hall-Héroult cell as seen looking in the long horizontal direction.

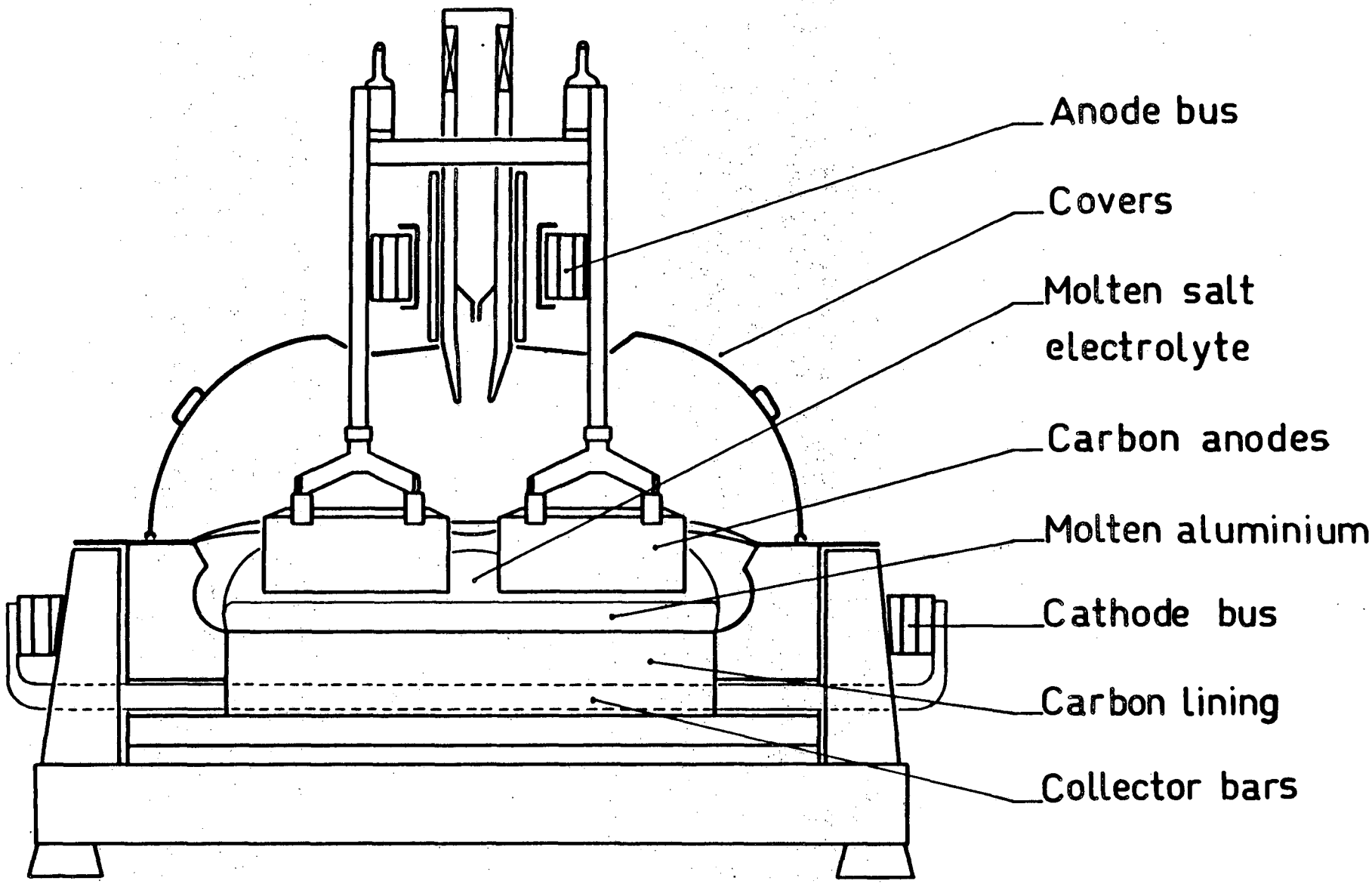

FIG. 2 Coordinates and main notations in a typical horizontal plane.

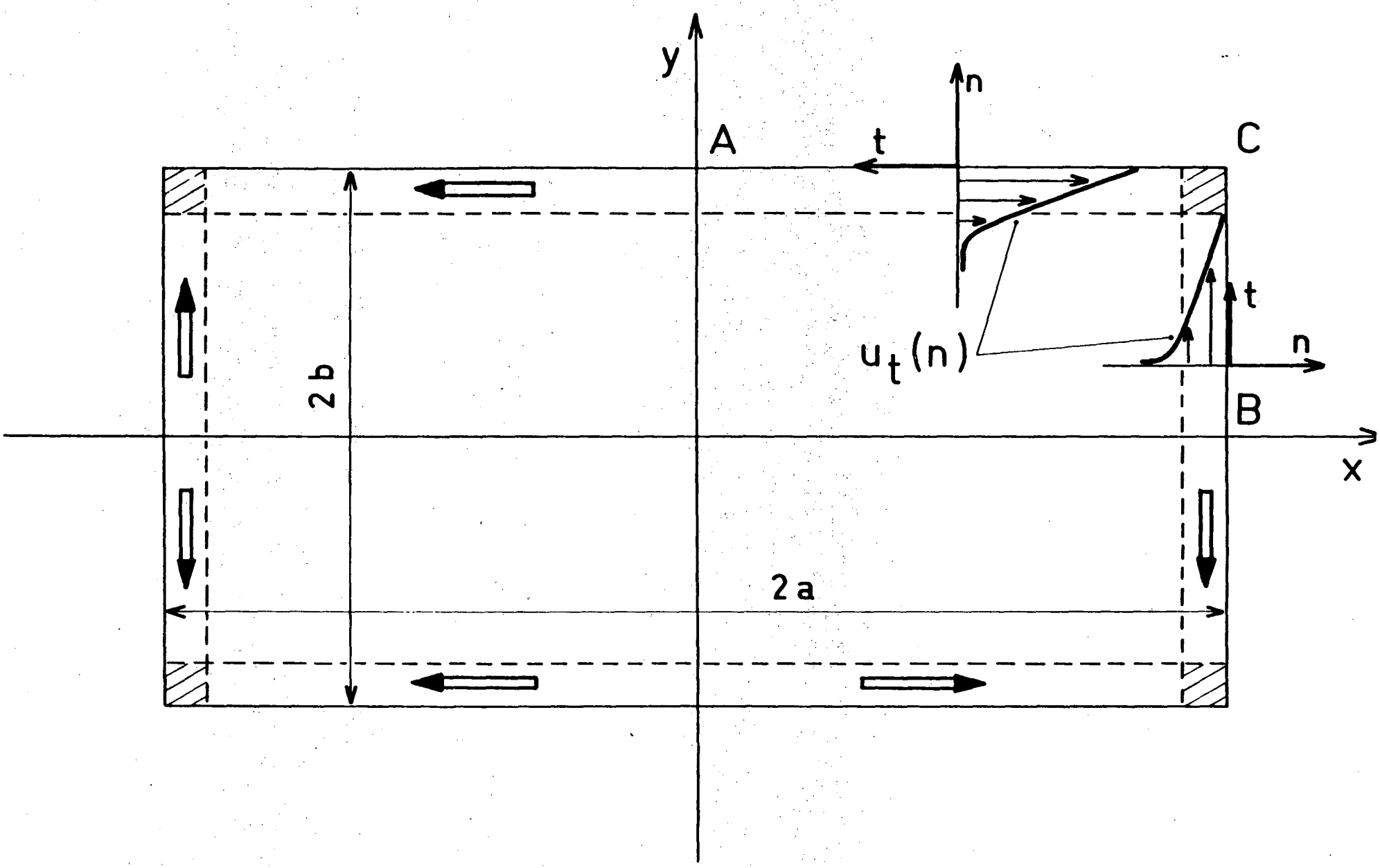

FIG. 3 Potential lines (G = Const.) of the $\langle \bar{j} \times \bar{B} \rangle$ force field, and pressure lines (P = Const.)

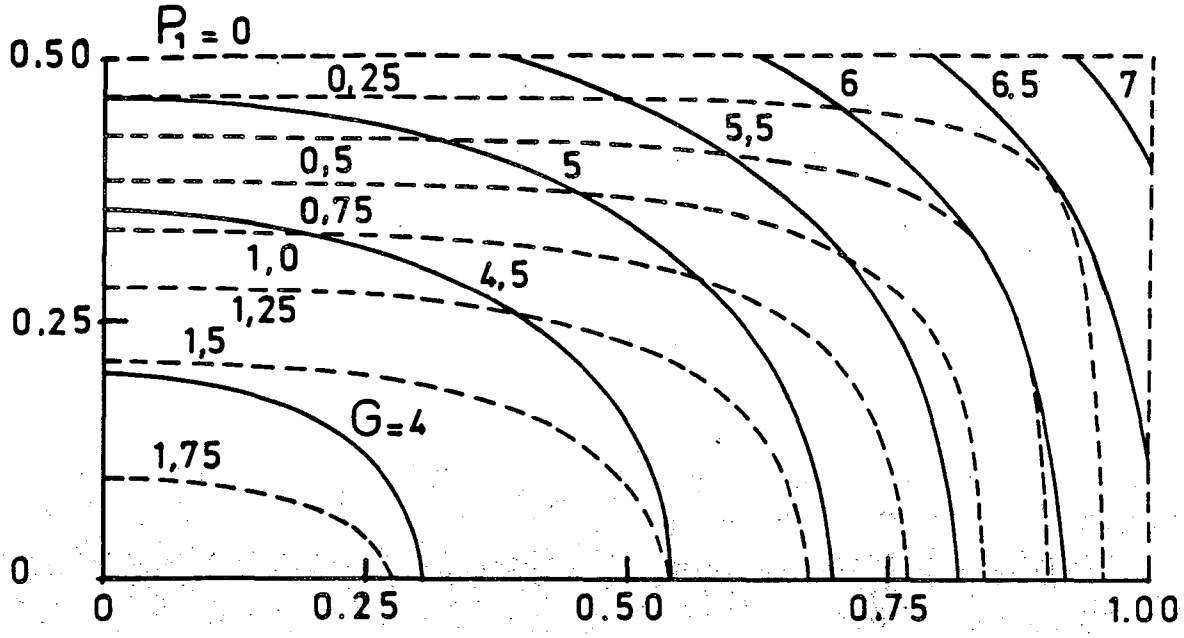

3 a) for a cell without central channel

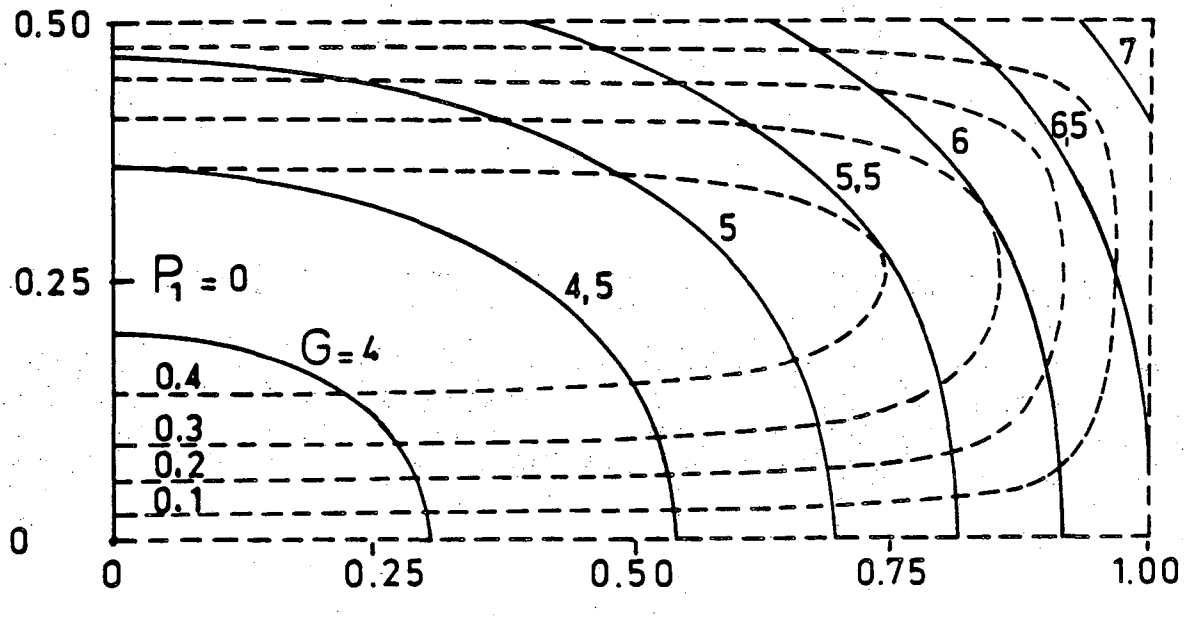

3 b) for a cell with central channel

FIG. 4 Streamlines of the cryolite flow underneath the anode.

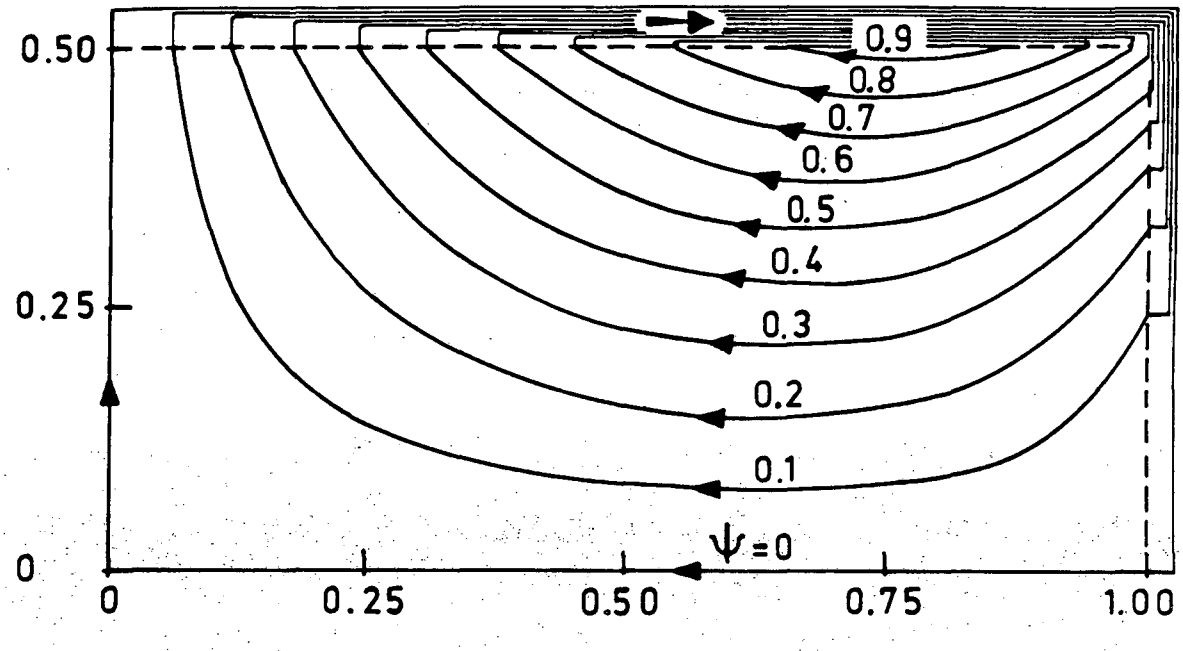

4 a) for a cell without central channel

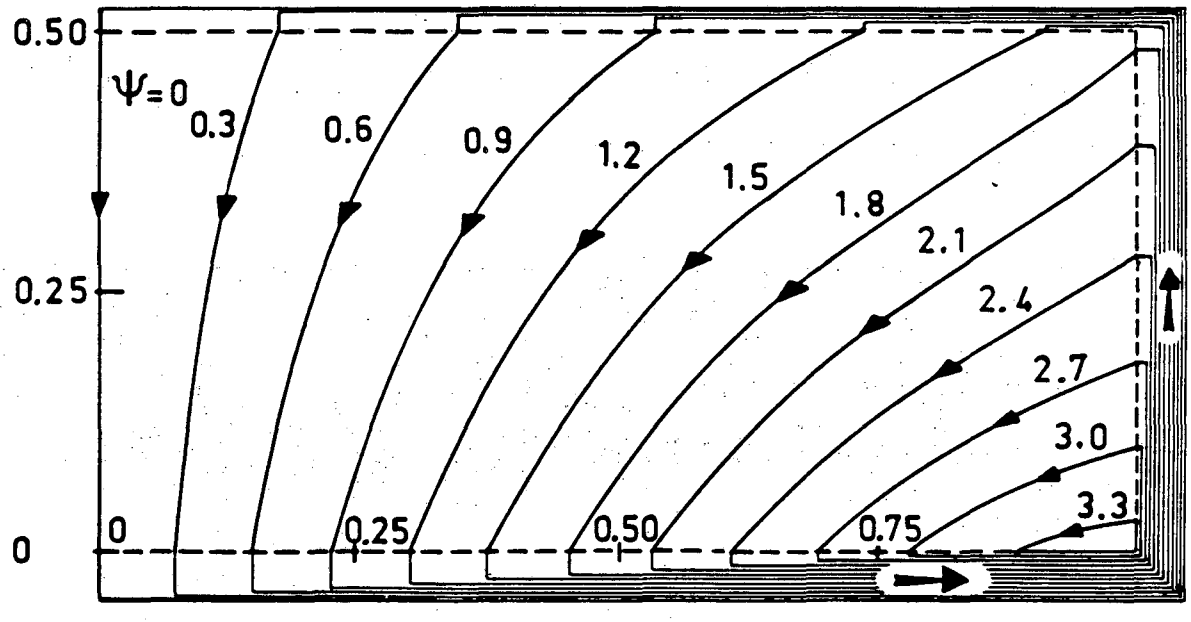

4 b) for a cell with central channel

FIG. 5 Interface contour lines when C = 1 (j_1 = 0, i.e., no horizontal current in the aluminum)

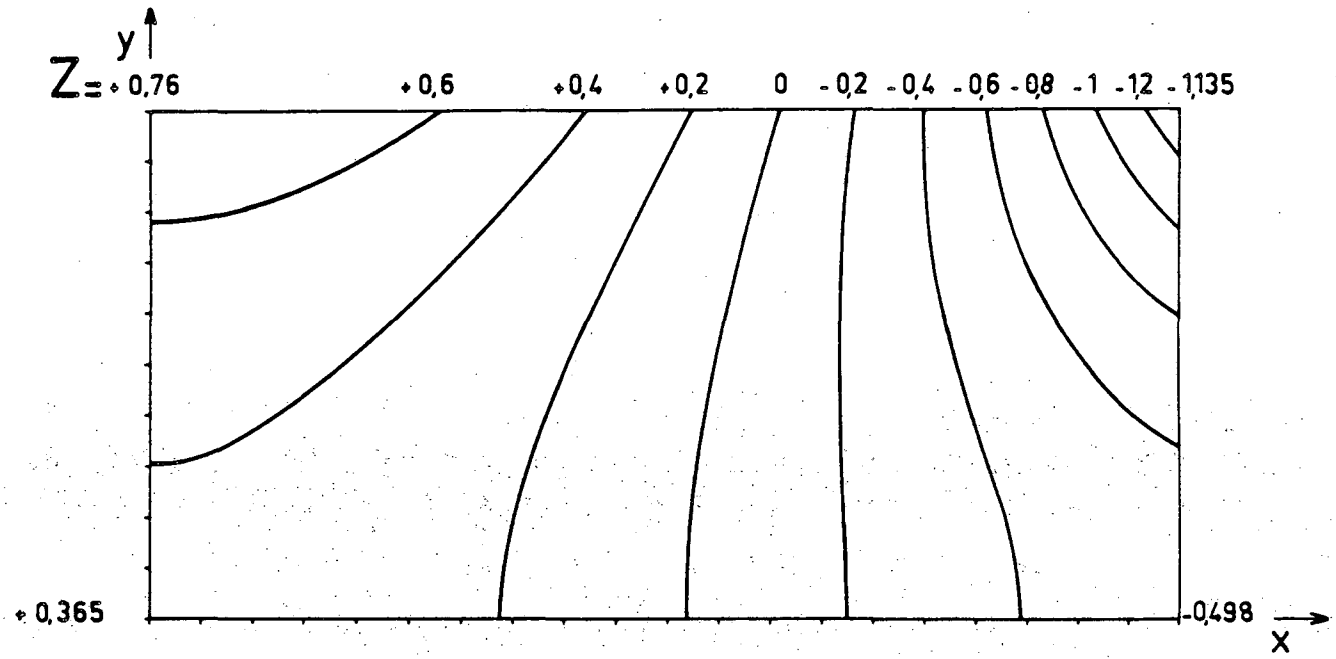

5 a) for a cell without central channel

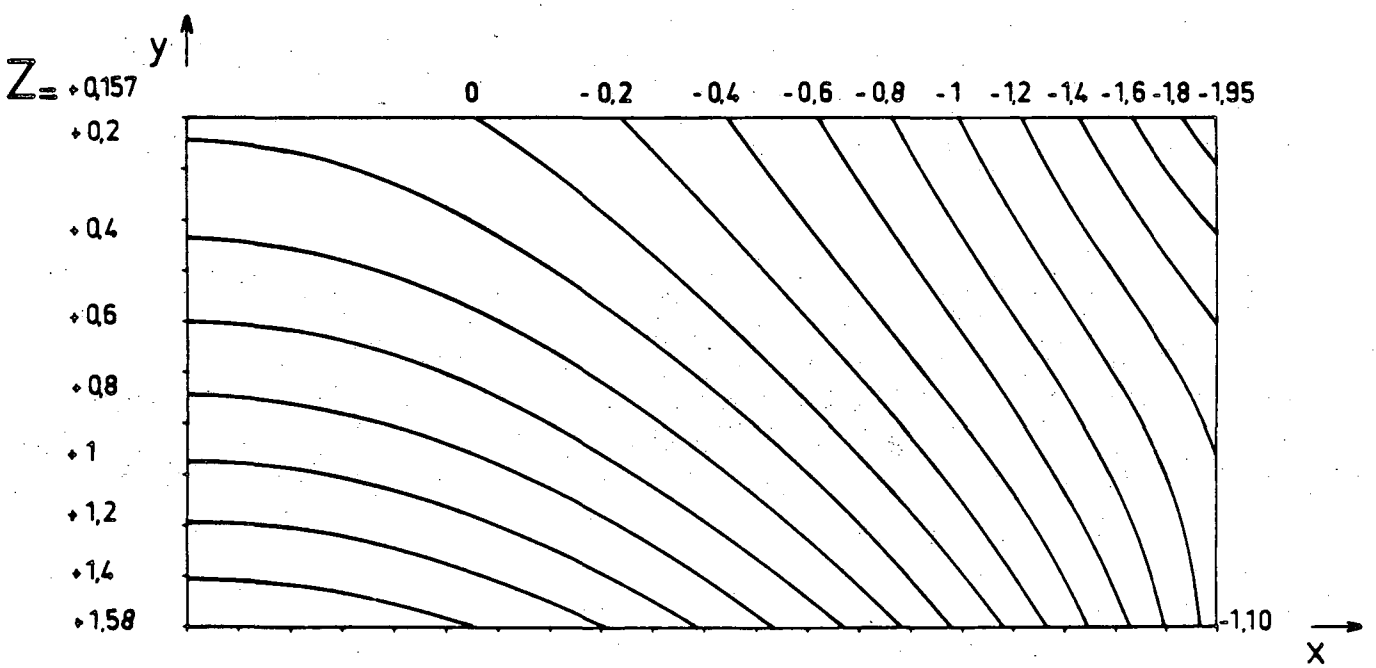

5 b) for a cell with central channel

FIG. 6 Interface contour lines when C = 0.5 (j_1/j_o = 0.634)

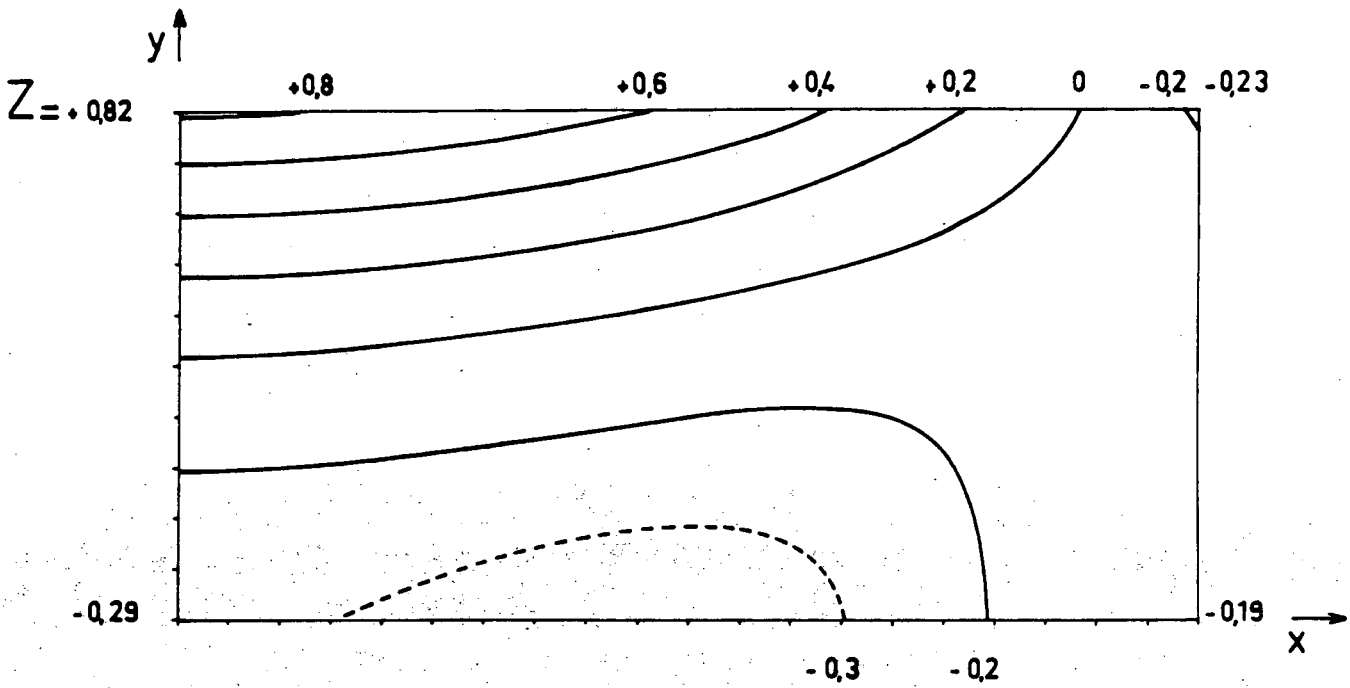

6 a) for a cell without central channel

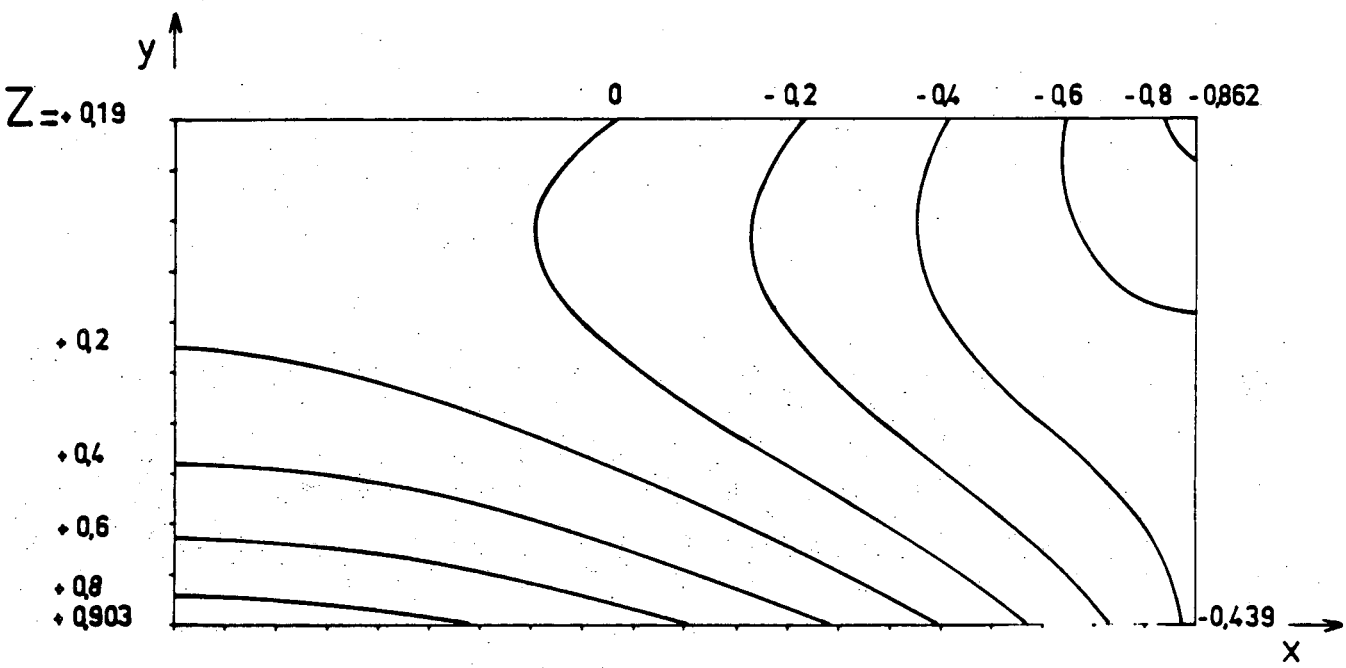

6 b) for a cell with central channel

FIG. 7 Interface shape in the four computed cases

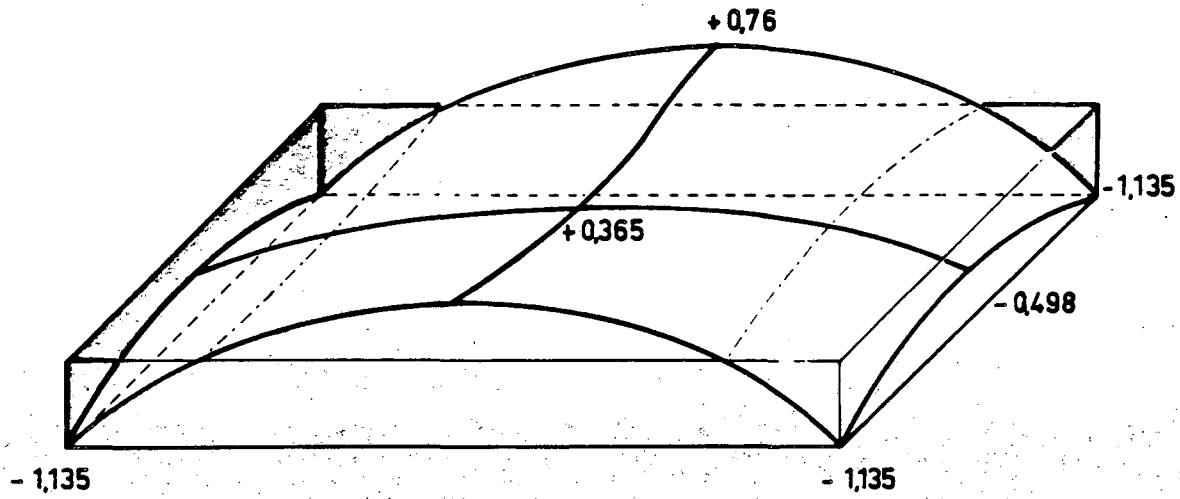

7 a) C = 1, without central channel

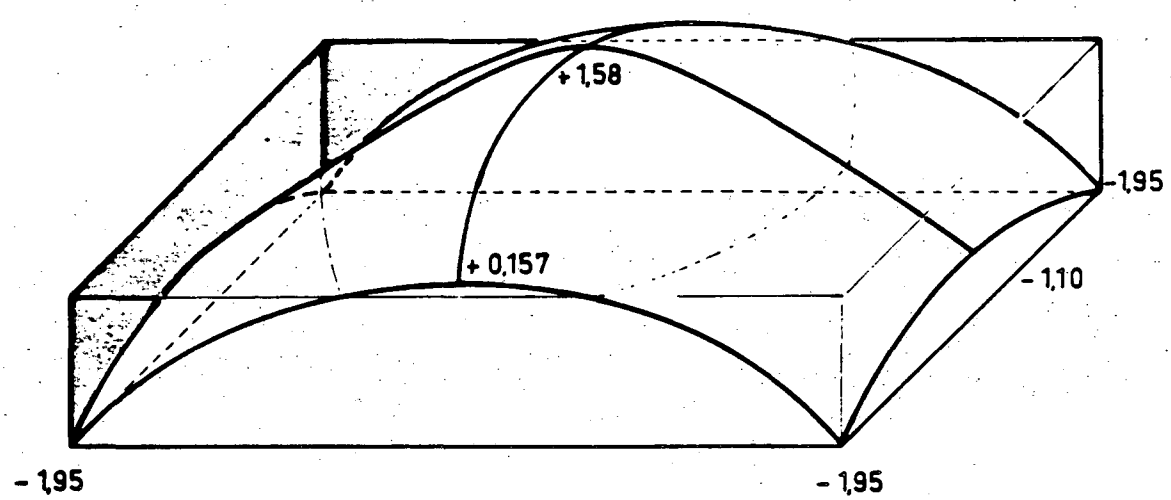

7 b) C = 1, with central channel

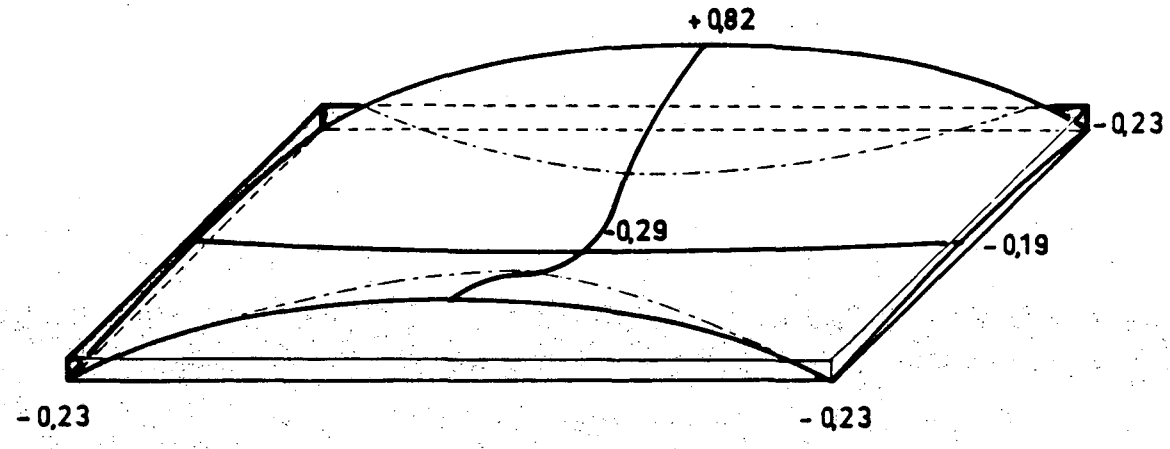

7 c) C = 0.5, without central channel

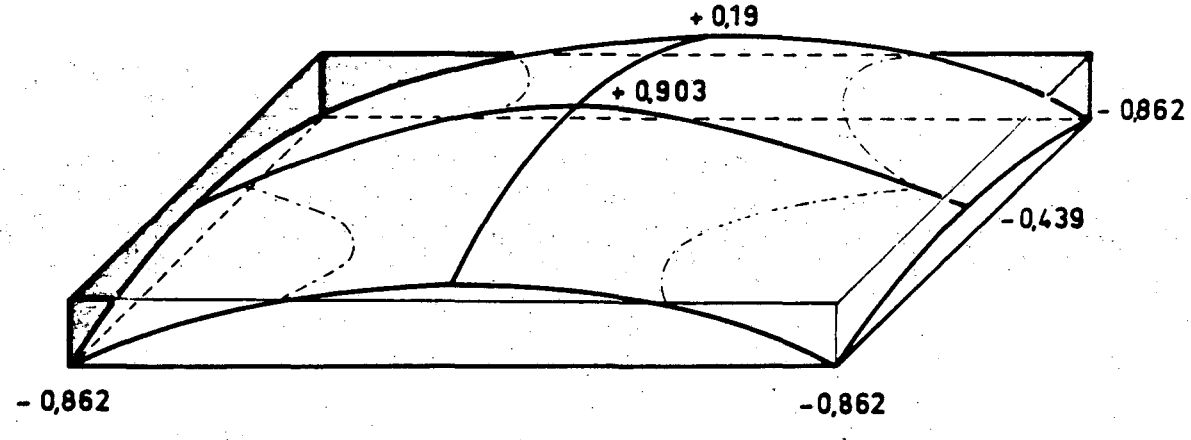

7 d) C = 0.5, with central channel

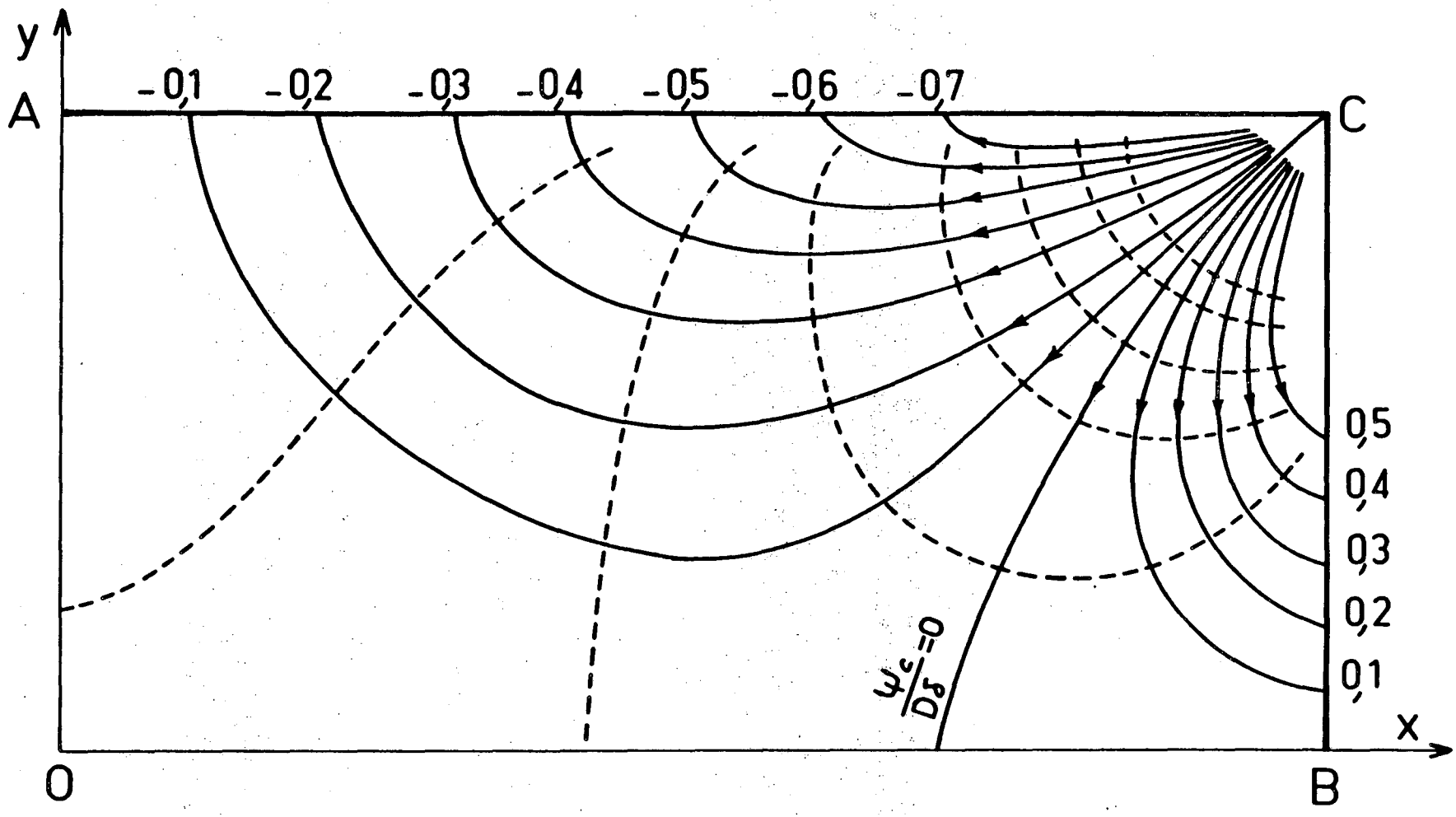

FIG. 8 Typical streamlines of the core flow feeding the side boundary layers in the aluminum pool.

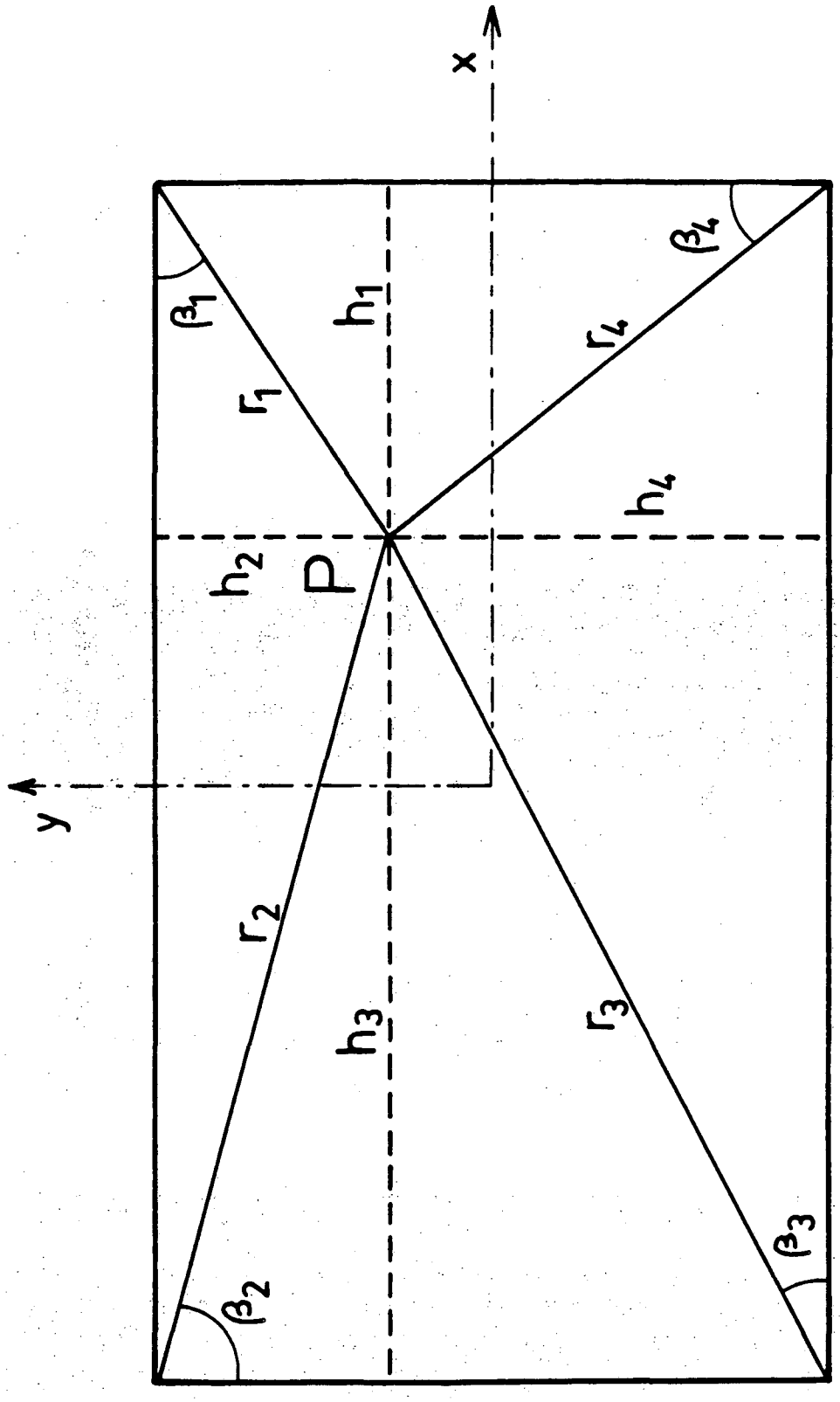

FIG. 9 Definitions of notations used in equation A1.

REFERENCES

1. S. D. Lympany, J. W. Evans and R. Moreau: "Magnetohydrodynamic effects in aluminum reduction cells," Proc. IUTAM Symp. "Metallurgical Applications of Magnetohydrodynamics," Cambridge, England. The Metals Soc., London 1983.

2. J. W. Evans, Y. Zundelevich and D. Sharma: "A Mathematical Model for Prediction of Currents, Magnetic Fields, Melt Velocities, Melt Topography and Current Efficiency on Hall-Heroult Cells," Met. Trans., 1981, vol. 12B, pp. 353-360.

3. S. D. Lympany and J. W. Evans: "The Hall-Heroult Cell: Some Design Alternatives Examined by a Mathematical Model," Met. Trans., 1983, vol. 14B, pp. 63-70.

4. E. Durand: "Electrostatique," Tome 1, 1964, Masson, p. 350.

5. H. S. Carslaw and J. C. Jaeger: "Conduction of Heat in Solids," 2nd ed., 1959, Clarendon Press, P. 171.

6. A. F. Johnson: "Light Metals 1978," vol. 1, pp. 45-58, The Metallurgical Society of AIME, N.Y.

7. J. P. Givry: Trans. Met. Soc. AIME, 1967, vol. 239, pp. 1161-1166.

8. C. Cercignani, G. Solinas, B. Crudelle, and R. Bacchiega: "Contribution to the Study of the Metal Flow Pattern in an Aluminum Electrolytic Cell," AIME Conference, 1977, paper no. 23.

This report was done with support from the Department of Energy. Any conclusions or opinions expressed in this report represent solely those of the author(s) and not necessarily those of The Regents of the University of California, the Lawrence Berkeley Laboratory or the Department of Energy.

Reference to a company or product name does not imply approval or recommendation of the product by the University of California or the U.S. Department of Energy to the exclusion of others that may be suitable.

TECHNICAL INFORMATION DEPARTMENT
LAWRENCE BERKELEY LABORATORY
UNIVERSITY OF CALIFORNIA
BERKELEY, CALIFORNIA 94720